Chemical Engineering Journal 259 (2015) 854–864

Contents lists available at ScienceDirect

Chemical Engineering Journal

journal homepage: www.elsevier.com/locate/cej

Simultaneous removal of lead and phenol contamination from water by nitrogen-functionalized magnetic ordered mesoporous carbon

Guide Yang [a,b], Lin Tang [a,b,*], Guangming Zeng [a,b,*], Ye Cai [a,b], Jing Tang [a,b], Ya Pang [c], Yaoyu Zhou [a,b], Yuanyuan Liu [a,b], Jiajia Wang [a,b], Sheng Zhang [a,b], Weiping Xiong [a,b]

[a] College of Environmental Science and Engineering, Hunan University, Changsha 410082, China
[b] Key Laboratory of Environmental Biology and Pollution Control, Hunan University, Ministry of Education, Changsha 410082, China
[c] Department of Biotechnology and Environmental Science, Changsha College, Changsha 410003, China

HIGHLIGHTS

- N-Fe/OMC was applied as a novel adsorbent to remove Pb(II) and phenol.
- The high capacities and fast rates for Pb(II) and phenol adsorption were observed.
- Partial complexation and competition between Pb(II) and phenol were verified.
- Excellent magnetic separation performance and effective reuse.

GRAPHICAL ABSTRACT

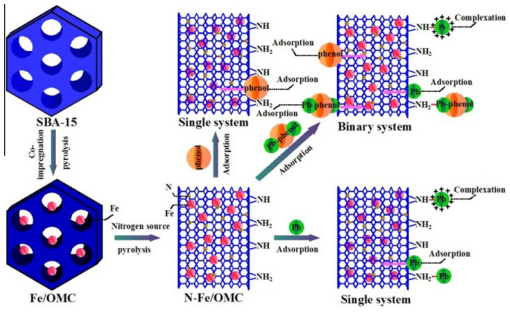

ARTICLE INFO

Article history:
Received 4 July 2014
Received in revised form 19 August 2014
Accepted 20 August 2014
Available online 27 August 2014

Keywords:
Lead
Phenol
Adsorption
Nitrogen-functionalized
Magnetic ordered mesoporous carbon

ABSTRACT

In this study, a novel nitrogen-functionalized magnetic ordered mesoporous carbon (N-Fe/OMC) with uniform pore size (3.8 nm) and excellent magnetic property (8.46 emu/g) was fabricated through simple impregnation then polymerization and calcination. The resultant adsorbent exhibited more preferential sorption toward Pb(II) and phenol than simple equivalent mixture of magnetic ordered mesoporous carbon (Fe/OMC) and pristine ordered mesoporous carbon (OMC). Binary adsorption showed that the coexistence of Pb(II) and phenol at low concentrations would slightly accelerate their jointly adsorption because of partial complexation between Pb(II) and phenol. While at high concentrations, Pb(II) adsorption would be inhibited in relation to the competition from phenol, but phenol adsorption was scarcely affected due to the directly phenol molecular adsorption pattern. Pb(II) adsorption was more suitable in alkaline solution and affected by ionic strength on account of electrostatic interaction, whereas phenol adsorption was better in neutral pH and hardly interfered by ionic strength as the adsorption was a physical combination process. Thermodynamics indicated that the uptakes of Pb(II) and phenol were endothermic and exothermic processes, respectively. Moreover, N-Fe/OMC could be regenerated effectively and recycled by using dilute NaOH and acetone solutions. These superior properties demonstrate that N-Fe/OMC is attractive for practical applications in treatment of water contamination by Pb(II) and phenol.

* Corresponding authors at: College of Environmental Science and Engineering, Hunan University, Changsha 410082, China. Tel.: +86 731 88822778; fax: +86 731 88823701.
E-mail addresses: tanglin@hnu.edu.cn (L. Tang), zgming@hnu.edu.cn (G. Zeng).

http://dx.doi.org/10.1016/j.cej.2014.08.081
1385-8947/

1. Introduction

Heavy metals and phenolic compounds are common pollutants in surface water and ground water, and pose a potential threat to the flora and fauna because of their toxicity, carcinogenicity and accumulation in the food chains [1,2]. For example, lead ions (Pb(II)) may cause stomachache, dysphoria, even cancer in human beings, and phenol also may contribute to nausea and skin corrosion. Additionally, heavy metals and phenolic compounds may occur together in contaminated water and soil, giving rise to more serious damage to the environment with their combined toxicity and relative mobility [3,4]. Such phenomenon commonly exists in printing, agricultural irrigation and plastic manufacturing. Consequently, finding effective ways to treat these pollutants, especially for their simultaneous removal has aroused worldwide interest recently. Among all possible techniques, adsorption is one of the most attractive approaches for heavy metals and phenolic compounds removal due to its high efficiency, simple and safe treating processes, versatility for different water systems and low cost [5]. Many adsorbents, including active carbons [6], chitosans [7], resins [8] and carbon nanotubes [4] have been applied for removal of heavy metals or/and phenolic compounds. However, there are some defects, such as low efficiency, bad stability and difficult separation, limiting their practical application.

Compared to traditional adsorbents, ordered mesoporous carbons (OMCs) with large surface area and pore volume, unique pore size, and excellent physicochemical and thermal stability are promising candidates in pollutant removal [9–11]. Whereas the adsorption behaviors of OMCs for specific pollutants, such as heavy metals and low molecular weight organic matters are often hindered due to the overlarge pore sizes and ordinary hydrophilicities. Previous studies demonstrated that transition elements, for example, metal nanoparticles of Co, Fe and Pt [12–14] or nonmetal atoms of N and P [15,16] can be utilized as catalysts to accomplish primary amorphous OMCs graphitization, strengthening their excellent acid-base stability, catalytic and hydrophilic properties. Besides, these transition elements introduction sometimes brings about some magical results. For example, introduction of magnetic nanoparticle of Fe can greatly improve their practical application in separation and reutilization [17], and introduction of nonmetal heteroatom of N element will equip OMCs with —NH_2 and —NH groups [18], boosting the chelation with heavy metals or organics.

According to the above considerations, it is supposed to triply improve the features of OMCs by incorporating with magnetic nanoparticles, and subsequently introducing nonmetal atoms to enhance and extend their physiochemical properties. Recently, similar functional carbon materials have been reported to be applied in the aspects of catalysis and electrochemistry [13,19]. But their outstanding abilities in adsorption and separation scarcely have been mentioned.

In this paper, a novel functional adsorbent, nitrogen-functionalized magnetic ordered mesoporous carbon (N-Fe/OMC) was prepared by adopting two-step method that primarily synthesizes magnetic ordered mesoporous carbon (Fe/OMC), and then followed by doping with nitrogen atoms using aniline as a nitrogen precursor and ammonium persulfate as an oxidant. After comprehensive characterization of its physicochemical properties, N-Fe/OMC is firstly used to investigate the removal behaviors of Pb(II) and phenol from wastewater. The single and binary adsorption systems were applied to investigate the distinct interaction of Pb(II) and phenol with N-Fe/OMC, and the complexation and competition between the two target pollutants, respectively. The effects of pH, ionic strength and temperature were studied, and the adsorption isotherms, kinetics and thermodynamics were proposed to analyze the adsorption mechanisms. The actual application was investigated by combining with the regeneration of N-Fe/OMC and its application in different water samples.

2. Materials and methods

2.1. Preparation of Fe/OMC

Mesoporous silicon templates (SBA-15) were prepared by hydrothermal synthesis method [20]. Fe/OMC was synthesized by following a co-impregnation method with slight alterations [21]. Typically, 1.0 g as-synthesized SBA-15 was impregnated with 10 mL multi-component alcohol solution containing 0.721 g $Fe(NO_3)_3{\cdot}9H_2O$ and 0.05 g oxalic acid, and then 2.0 mL furfuryl alcohol was added dropwise into the above mixture. After that, the mixture thus prepared was heated at 90 °C for 10 h in air and calcinated at 900 °C for 2 h under flowing nitrogen atmosphere. After dissolving the silica framework with 2.0 mol/L NaOH solution at 90 °C, the resultant solid was filtered, washed, dried and then stored in a nitrogen-filled glovebox until required. For comparison, OMC was also prepared without iron.

2.2. Preparation of N-Fe/OMC

N-Fe/OMC was synthesized as follows: 1.0 g Fe/OMC nanocomposite was first dissolved into 300 mL 0.1 mol/L HCl under 3.0 h mechanically stirring, and subsequently 1.0 mL aniline was in situ polymerized using 2.5 g ammonium persulfate as the initiator and HCl as the catalyst. The polymerization was conducted in an ice bath (<5 °C) for 24 h. Then the samples were repeatedly washed with 50 wt% ethanol solution and dried at 60 °C overnight. After carbonization the immature nanocomposites at 950 °C for 3 h under nitrogen atmosphere, the synthetic N-Fe/OMC was acquired.

2.3. Characterization

Transmission electron microscopy (TEM, JEOL JEM-1230) and Scanning electron microscope (SEM, JEOL JSM-6700) images were used to investigate the morphology and structure of N-Fe/OMC. The Energy dispersive X-ray (EDX) analysis in the SEM image was applied to detect the element composition of the resultant sample. X-ray diffraction (Rigaku D/max-II B) and FTIR spectrometer (Nicolet NEXUS 670) were applied to analyze the likely existence of compositions and functional groups. Nitrogen adsorption measurements at 77 K were performed using an ASAP 2020 volumetric adsorption analyzer. Raman spectroscopy was mounted by using a LabRam HR800 Raman spectrometry. X-ray photoelectron spectroscopy (XPS, Thermo Fisher Scientific, UK) was proposed to analyze the surface elemental composition. Zetasizer Nano (ZEN3600, Malvern) and vibrating sample magnetometer (VSM National Institute of Metrology) were used to determine the zeta potential and magnetization of the samples, respectively.

2.4. Batch adsorption experiments

Adsorption of Pb(II) and/or phenol on N-Fe/OMC were performed in 50-mL stoppered conical flasks undergoing shaking at 150 rpm in a water bath shaker. 0.1 mol/L HCl or NaOH was used to adjust the solution pH, and NaCl was used as a function of ionic strength. Before each experiment, 5 mg of specific mesoporous adsorbent was dispersed into 10 mL of homogeneous aqueous solution containing certain amount of NaCl. At each preselected time point, the solid and liquid phases were separated using an external magnet for magnetic OMC or centrifugation for OMC, and then the supernatant was filtered through 0.45-μm membrane for measurement of the residual pollutant concentrations.

Pb(II) concentration was determined by a Perkin–Elmer Analyst 700 atomic absorption spectrophotometer (AAS, Perkin-Elmer, USA), and phenol was determined on a UV–vis spectrophotometer (UV-754N shanghai, China) at 274 nm. All measurements were performed in triplicate, and average values and standard deviations were presented. The amount of adsorbed Pb(II) or phenol was calculated by Eq. (1):

$$Q_e = \frac{(C_0 - C_e) \times V}{m} \quad (1)$$

where Q_e was the equilibrium adsorption capacity (mg/g); C_0 and C_e were the initial and equilibrium concentration of Pb(II) or phenol in solution (mg/L), respectively; V was the volume of aqueous solution (mL) and m was the mass of adsorbent used (mg).

2.5. Regeneration and reuse experiments

The feasibility of regenerating N-Fe/OMC for reuse was investigated by using dilute NaOH and acetone solutions. Specifically, after accomplishment of the adsorption experiments, the Pb(II)-loaded (or phenol-loaded) adsorbent was magnetically separated and subsequently added into 10 mL 0.2 mol/L NaOH solution (or 20% acetone solution) for desorption at 150 rpm at 30 ± 1 °C for 24 h. After washing thoroughly with ultrapure water to neutrality, the regenerated adsorbent was recycled and reused, and the adsorption performance of N-Fe/OMC was investigated again.

2.6. Application in real water samples

Four different water samples were applied to investigate the actual application of N-Fe/OMC. Specifically, 5 mg N-Fe/OMC was added into different initial concentrations of Pb(II) and/or phenol solution for adsorption test at 150 rpm at 30 ± 1 °C for 240 min. Then, the residual Pb(II) and phenol concentrations were determined by AAS and UV–vis spectrophotometer, respectively. The Pb(II) and phenol stock solutions were prepared using ultrapure water, tap water, river water and landfill leachate. River water and landfill leachate samples were acquired from Xiang River (Changsha, China) and Heimifeng Refuse Landfill (Changsha, China), respectively.

3. Results and discussion

3.1. Characterization of materials

SEM images revealed that the mesoporous sample consisted of many rope-like domains with relatively uniform lengths of 0.8 μm or so, which were aggregated into wheat-like macrostructures (Fig. 1a and b). The EDX analysis in the SEM image indicated that the presence of iron and nitrogen elements on N-Fe/OMC surface, and the relevant EDX image and elements percentages of the resultant sample were shown in the inset of Fig. S1 and Table S1, respectively in the Supporting Information. TEM images showed that N-Fe/OMC had well-ordered mesopore arrays and 2D hexagonal pore structure (Fig. 1c and d). Fig. 1c showed that the distance between mesopores was approximately 10.2 nm, and the nanoparticles with an average diameter about 14 nm were dispersed on the carbon matrix. These nanoparticles were α-Fe, Fe_3O_4 and γ-Fe_2O_3 particles, and the details could be seen in XRD diffraction patterns (Fig. S2). The iron nanoparticles were in situ formed during the first calcinations and could be found clearly in the Fig. 1d, inset. Fig. 1d also showed that after incorporation of iron nanoparticles and nitrogen atoms, the mesoporous adsorbent was been partly graphitized.

Raman spectra of Fe/OMC and N-Fe/OMC show that the two mesoporous adsorbents both possess D mode peak and G mode peak, which are near 1349 cm^{-1} and 1593 cm^{-1}, respectively (Fig. 2a). D mode is corresponding to the disordered sp^2-hybridized carbon atoms while G mode is related to the structural integrity of sp^2-hybridized carbon atoms of ordered mesoporous carbons [22]. The ratio between the disorder and graphite area bands (I_D/I_G) is interpreted as a measure of the degree of the material's orderliness and graphitization. As seen, the I_D/I_G ratio of N-Fe/OMC (0.941) is lower than that of Fe/OMC (1.055), indicating that the graphitization of degree of N-Fe/OMC outweighs than that of Fe/OMC. FTIR spectra of three samples were used to assess the functional groups of three nanoparticles (Fig. 2b). The broad band centered at about 3400 cm^{-1} can be assigned to the O—H stretching vibration for OMC and Fe/OMC, and N—H stretching combined with O—H vibration model for N-Fe/OMC [23]. The common peaks at 1120 cm^{-1} for three nanoparticles correspond to C—O stretching vibration [17], which is the skeleton structure of these mesoporous carbons. The band at 1640 cm^{-1} is attributed to the O—H deformation of water or C=O stretching vibration observed in OMC and Fe/OMC, which translated into N—H vibration coupled with C—N stretching mode (1630 cm^{-1}) after incorporation with nitrogen [24]. The peaks at 570 cm^{-1} in Fe/OMC (b) and N-Fe/OMC (c) spectra are attributed to the Fe—O bond vibration, demonstrating that magnetic iron nanoparticles were successfully introduced in or on the OMC matrix [25]. For N-Fe/OMC spectrum, the peaks located at 2225 and 1348 cm^{-1} were assigned to the C≡N stretching vibration and the C—N stretching vibration, respectively, which were shaped during the second calcination process [24].

The isotherm curves of Fe/OMC and N-Fe/OMC (Fig. 3) shows representative type-IV curves with H1 hysteresis loops in the P/P_0 range 0.4–0.8, indicating the uniform mesoporous sizes of mesoporous samples. The pore-size distribution curves (Fig. 3, insert) confirmed after incorporating with nitrogen atoms, the pore size decreased from 4.9 to 3.8 nm. The reduction was probably related to nitrogen entering into channels, combining with the inherent carbon of the carbon matrix and partially occupying or blocking mesopores. Given that the sizes of lead ions and phenol molecules were centered at 0.1–0.2 and 0.6–0.7 nm, respectively, the decrease in pore size is more propitious to pollutants removal. The BET surface areas of Fe/OMC and N-Fe/OMC were 523 and 886 m^2/g, respectively. This increase was probably because of the occurring of C—N structures during the second pyrolysis process, which generated new sites and thereby aggrandized the surface area.

The magnetic behavior of the N-Fe/OMC nanocomposite was shown in Fig. 4. The extremely weak hysteresis revealed that the sample was close to superparamagnetic (no remanence remained once the applied magnetic field was removed). The saturation magnetization (Ms) of the resultant sample was 8.46 emu/g, which indicated that N-Fe/OMC could be easily separated from aqueous solution using high density magnet.

XPS spectra of N-Fe/OMC indicated that iron and nitrogen atoms were successfully introduced into OMC (Fig. S3 and Table S1). The water-solubility and acid-base stability tests indicated that N-Fe/OMC was highly hydrophilic and more stable in alkaline than acidic condition, respectively (Fig. S4 and Table S2).

3.2. Single and binary adsorption

The sorption isotherms of Pb(II) and phenol on three samples were shown in Fig. 5a and b. The Pb(II) adsorption capacities were in the following order: N-Fe/OMC > Fe/OMC > OMC (Fig. 5a), indicating the enhanced adsorption capacity of OMC by magnetic iron nanoparticles and nitrogen atoms incorporation. Specifically, the modification not only imports the additional adsorption sites

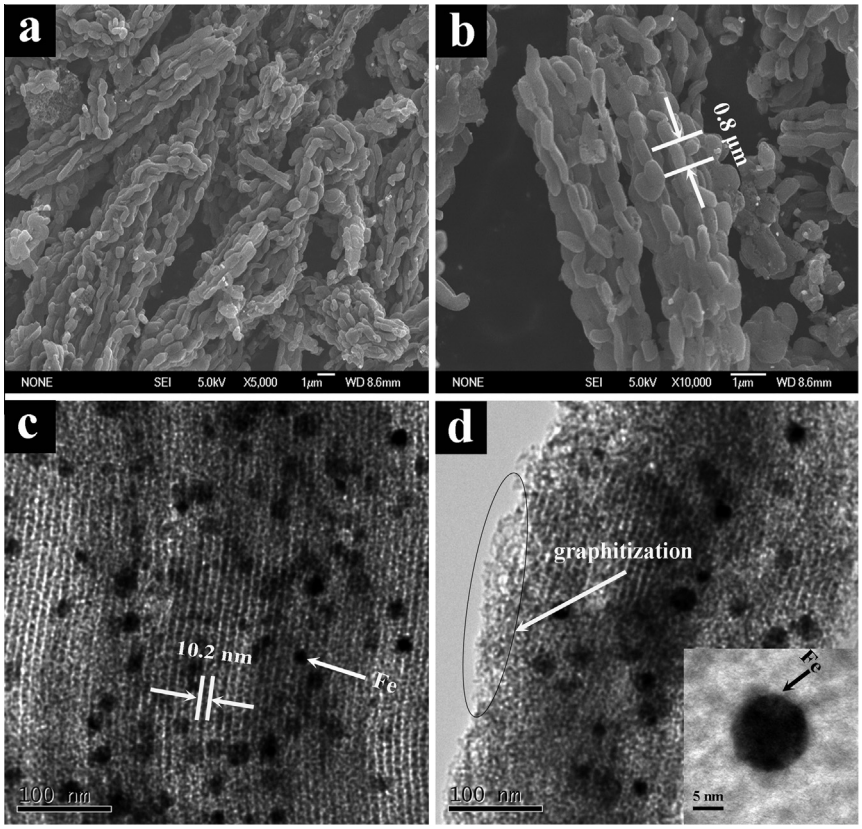

Fig. 1. SEM (a and b) and TEM (c and d) images of N-Fe/OMC.

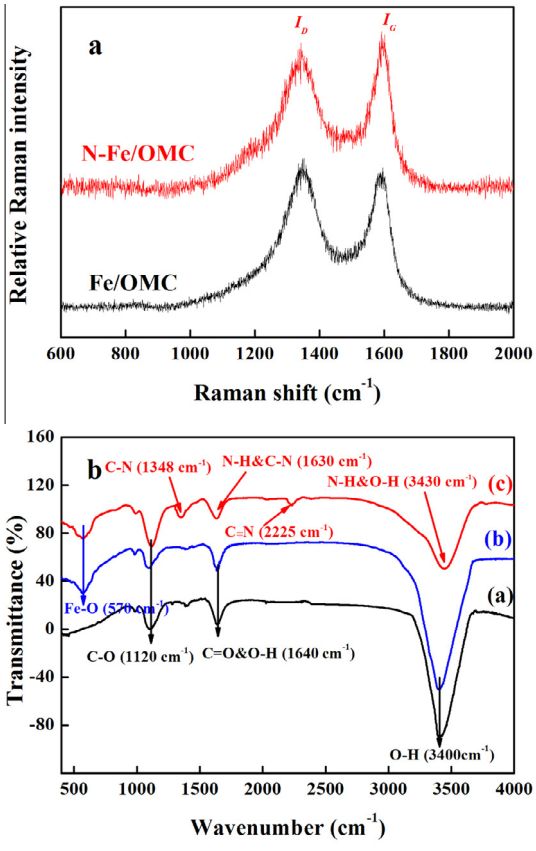

Fig. 2. Raman spectra (a) of Fe/OMC and N-Fe/OMC and FTIR spectra (b) of OMC, Fe/OMC and N-Fe/OMC.

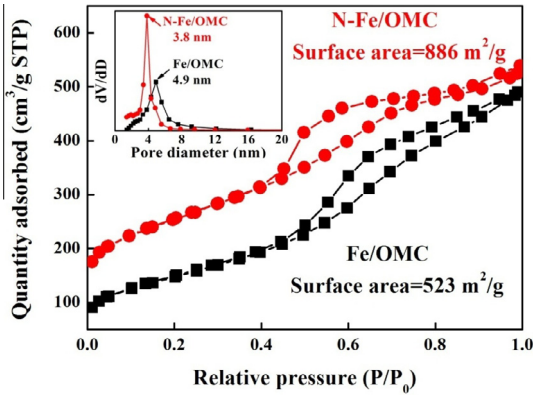

Fig. 3. N_2 sorption isotherms with inset the corresponding pore distribution curves of mesoporous carbon Fe/OMC and N-Fe/OMC.

provided by the oxygen atoms of iron oxide nanoparticles on the surface of OMCs [26], but also produces —NH_2 and —NH functional groups, chelating strongly with targeted Pb(II). While for phenol adsorption, the maximum sorption amounts of three adsorbents were all not less than 160 mg/g (Fig. 5b). This was ascribed to the high surface areas and unique mesopores of mesoporous samples. The almost same sorption capacities of three mesoporous adsorbents indicated that the functionalization had no obvious effect on phenol adsorption, and the uptake of phenol was probably dependent only on the available pores of N-Fe/OMC. The slightly better for phenol adsorption on N-Fe/OMC was connected with the structure of N-Fe/OMC since the pore size became smaller and the surface area got higher after the modification.

Langmuir model was applied to describe isotherm data. The relevant isotherm equation was represented as Eq. (2):

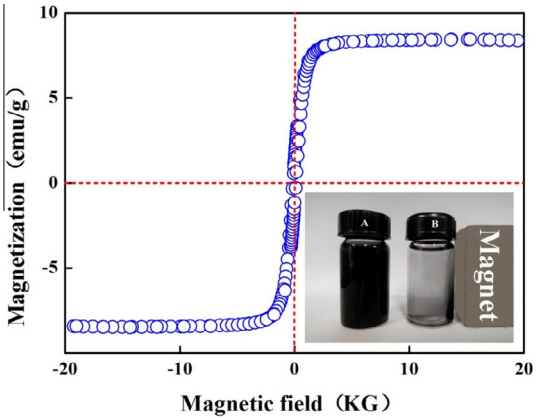

Fig. 4. Magnetization curve of N-Fe/OMC.

$$Q_e = \frac{Q_m K_L C_e}{1 + K_L C_e} \quad (2)$$

where Q_m (mg/g) was the maximum amount of adsorption corresponding to the monolayer coverage, and K_L (L/mg) was the Langmuir constant related to the adsorption energy. The corresponding values of Q_m, K_L and correlation coefficients (R^2) for Langmuir isotherm were listed in Table 1. As seen, the adsorption data of three mesoporous adsorbents for Pb(II) and phenol were both fitted commendably with Langmuir isotherm model, assuming that the adsorbed Pb(II) and phenol formed monolayer coverage on the adsorbent surface and all sorption sites were equal with uniform adsorption energies without any interaction between the adsorbed substances [27,28]. For Pb(II), the maximum adsorption amount of N-Fe/OMC was 159.93 mg/g, which was obviously superior to OMC (113.79 mg/g) and Fe/OMC (136.11 mg/g). For phenol, the maximum adsorption amounts were all around 180 mg/g. The above excellent sorption performance indicated that N-Fe/OMC had great advantage in Pb(II) and phenol adsorptive removal from wastewater.

The mutual effects of coexisting Pb(II) and phenol on adsorption of each other were evaluated and the results were shown in Fig. 5c and d. In comparison with the single system, the coexistence of Pb(II) and phenol at low concentrations (25 mg/L) slightly accelerated their jointly adsorption. While at high concentrations, the Pb(II) adsorption was inhibited, but the uptake of phenol almost maintained the same level as no addition. The large difference suggested different mechanisms between Pb(II) and phenol adsorption onto N-Fe/OMC. A complexation interaction would probably occur between Pb(II) and phenol. Specifically, in addition to the original adsorption, an ion exchange occurred between Pb(II) and hydrogen atoms on the hydroxy groups of phenol molecules, which consequently formed Pb(II)-phenol complexes and were finally adsorbed on the adsorbent surface or chelated with —NH and —NH_2 groups. Thus more Pb(II) and phenol would be adsorbed on N-Fe/OMC hybrids at lower concentrations. However, the complex reaction was limited to a handful of Pb(II) and phenol molecules. As phenol concentration increased, excessive phenol could compete with Pb(II) for the available adsorption sites on N-Fe/OMC, and thus suppressed obviously the uptake of Pb(II). This effect was not obvious on phenol adsorption with addition of high concentration of Pb(II), which was probably ascribed to the uptake of phenol onto N-Fe/OMC by the molecular form [29].

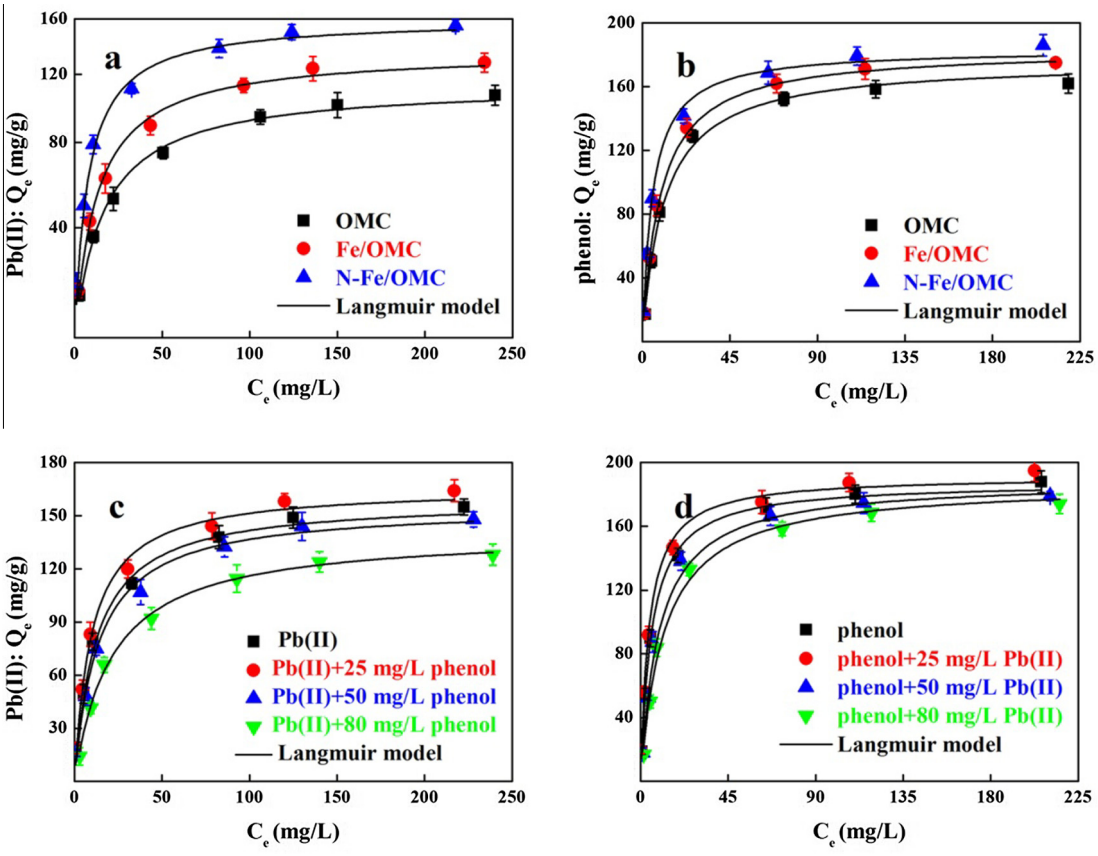

Fig. 5. The adsorption isotherms for Pb(II) and phenol removal on three different adsorbents (OMC, Fe/OMC and N-Fe/OMC) in the single system (a and b) and on N-Fe/OMC in the binary system (c and d). Adsorbents dose of 5 mg, pH 7.0, temperature of 30 ± 1 °C, contact time of 240 min and ionic strength of 0.01 mol/L NaCl.

Table 1
The parameters for the Langmuir adsorption isotherms of Pb(II) and phenol on N-Fe/OMC (OMC and Fe/OMC) in single system or binary system.

Water environment	Adsorbent/addition	Pb(II)			Phenol		
		K_L (L/mg)	Q_m (mg/g)	R^2	K_L (L/mg)	Q_m (mg/g)	R^2
Single system	OMC	0.042	113.79 ± 3.29	0.995	0.089	175.96 ± 6.51	0.991
	Fe/OMC	0.052	136.11 ± 3.61	0.996	0.108	183.71 ± 1.52	0.999
	N-Fe/OMC	0.083	159.93 ± 5.24	0.987	0.113	185.51 ± 4.43	0.995
Binary system	25 mg/L phenol + Pb(II)	0.102	166.01 ± 7.63	0.989	/	/	/
	50 mg/L phenol + Pb(II)	0.058	156.03 ± 7.34	0.991	/	/	/
	80 mg/L phenol + Pb(II)	0.032	141.12 ± 7.81	0.995	/	/	/
	25 mg/L Pb(II)+phenol	/	/	/	0.241	189.42 ± 5.02	0.993
	50 mg/L Pb(II)+phenol	/	/	/	0.108	183.33 ± 3.75	0.995
	80 mg/L Pb(II)+phenol	/	/	/	0.089	181.95 ± 6.34	0.991

Table 2
The comparison of removal performance of various adsorbents used for Pb(II) removal.

Adsorbent	Q_m (mg/g)	Equilibrium time	Isotherm model	Adsorption condition	References
Graphene nanosheets	35.46	60 min	Langmuir model	pH = 4.0, T = 30 °C	[30]
Imprinted polymer supported by SBA-15	38.01	90 min	Langmuir model	pH = 6.0, T = 25 °C	[31]
Iron oxide coated sepiolite	119.34	>1 h	Langmuir model	pH = 5.0, T = 45 °C	[32]
Acidic cation resin	65.4	360 min	Koble–Corrigan model	pH = 5.0	[33]
Porous $NiFe_2O_4$ adsorbent	48.98	60 min	Langmuir and Sips models	pH = 5.0, T = 35 °C	[34]
Manganese oxide coated zeolite	74.52	180 min	Langmuir and Redlich–Peterson model	pH = 4–6, T = 45 °C	[35]
Titanium dioxide/carbon nanotube composites	137	60 min	Langmuir model	pH = 6.0, T = 25 °C	[36]
OMC	113.79	60 min	Langmuir model	pH = 7.0, T = 30 °C	This study
Fe/OMC	136.11	60 min	Langmuir model	pH = 7.0, T = 30 °C	This study
N-Fe/OMC	159.93	60 min	Langmuir model	pH = 7.0, T = 30 °C	This study

Table 3
The comparison of removal performance of various adsorbents used for phenol removal.

Adsorbent	Q_m (mg/g)	Equilibrium time	Isotherm model	Adsorption condition	References
SWCNTs/calcined-sepiolite	155.8	48 h	Langmuir model	T = 30 °C	[37]
Manganese nodule leached residue	100.00	4 h	Langmuir model	pH = 7.7, T = 25 °C	[38]
Starch-derived starbon S800	100.4	24 h	Langmuir model	T = 25 °C	[39]
Activated carbon (ACK1)	17.83	240 min	Langmuir model	pH = 7.0, T = 25 °C	[40]
Magnetic porous carbon microspheres	35	10 h	/	pH = 7.0, T = 25 °C	[41]
Magnetic mesoporous carbon (FePt@C-L-700)	139	10 h	/	pH = 7.0, T = 25 °C	[42]
Modified natural red clay (HDTMA-clay)	11.28	6 h	Langmuir–Freundlich model	pH = 5.8, T = 20 °C	[43]
OMC	175.96	90 min	Langmuir model	pH = 7.0, T = 30 °C	This study
Fe/OMC	183.71	90 min	Langmuir model	pH = 7.0, T = 30 °C	This study
N-Fe/OMC	185.51	90 min	Langmuir model	pH = 7.0, T = 30 °C	This study

The corresponding values of Langmuir isotherm model in binary system were also listed in Table 1. The results showed that Langmuir isotherm model was suitable for description of Pb(II) and phenol removal with high correlation coefficients R^2. Meanwhile, the maximum adsorption amounts for Pb(II) decreased significantly with the increase of phenol, while for phenol, it almost kept stable with Pb(II) increase. Such phenomenon again proved distinct adsorption mechanisms between Pb(II) and phenol with N-Fe/OMC in the binary system: complexation and competition for Pb(II), while only slight complexation for phenol. In addition, compared with other adsorbents [30–43], shown in Tables 2 and 3, N-Fe/OMC also exerted excellent adsorptive removal performance towards Pb(II) and phenol in adsorption capacity, equilibrium time and adsorption conditions.

3.3. Effect of pH

Adsorption of Pb(II) and phenol on N-Fe/OMC as a function of contact time at different pH were presented in Fig. 6a and b. The Pb(II) and phenol adsorption were both rapid in their infancy and then slowed down gradually till reaching sorption equilibrium. The equilibrium time and efficiencies for Pb(II) and phenol sorption were approximately 60 min, 80% and 90 min, 90% respectively. Two common kinetic models, pseudo-first-order and pseudo-second-order models are applied to decrease the adsorption process. The corresponding equations are listed as follows:

$$\frac{dQ_t}{dt} = K_1(Q_e - Q_t) \tag{3}$$

$$\frac{dQ_t}{dt} = K_1(Q_e - Q_t)^2 \tag{4}$$

where Q_e and Q_t (mg/g) are the adsorption capacities of N-Fe/OMC towards Pb(II) and phenol at equilibrium and time t (min), respectively; K_1 (min^{-1}) and K_2 (g/mg min) are the related rate constants, respectively. The relevant kinetic parameters were listed in Table 4. It could be found that the data of Pb(II) adsorption could be better described by the pseudo-second-order model, whereas phenol adsorption could be well fitted with both of pseudo-first-order and pseudo-second-order models. Such results indicated Pb(II) adsorption was related to the chemisorption rate-controlling mechanism [1], while phenol removal was probably related to mesoporous structures on the N-Fe/OMC [29].

The change of pH had different effects on Pb(II) and phenol adsorption. For Pb(II), the adsorption rate and efficiency increased gradually as pH increases from 3.05 to 8.12 (Fig. 6a). The sorption

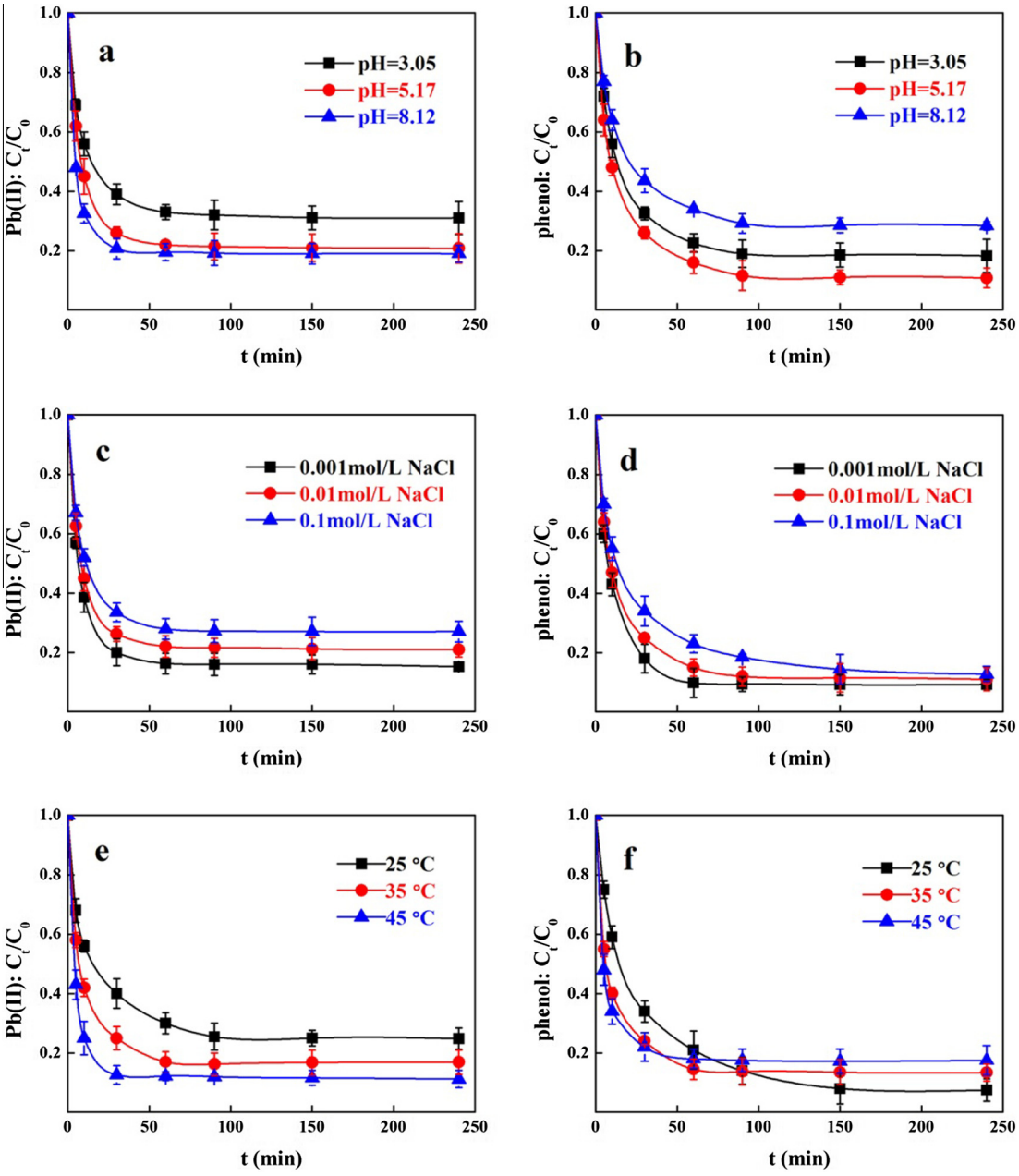

Fig. 6. Removal of Pb(II) and phenol as a function of contact time at different pH values (a and b), different ionic strengths (c and d) and different temperatures (e and f), respectively. Initial Pb(II) and phenol concentrations of 50 mg/L and 50 mg/L, respectively, and adsorbent dose of 5 mg.

Table 4
Kinetic model parameters for the adsorption of Pb(II) and phenol onto N-Fe/OMC at different pH values.

Pollutants	pH values	Pseudo-first-order			Pseudo-second-order		
		K_1 (g/mg/min)	Q_e (mg/g)	R^2	K_2 (min^{-1})	Q_e (mg/g)	R^2
Pb(II)	3.05	0.110	67.43 ± 2.24	0.955	0.0028	70.82 ± 3.52	0.995
	5.17	0.126	78.16 ± 3.26	0.972	0.0034	80.77 ± 2.42	0.999
	8.12	0.198	80.42 ± 2.52	0.968	0.0074	81.77 ± 2.85	0.999
Phenol	3.05	0.077	79.99 ± 2.25	0.995	0.0015	85.18 ± 3.12	0.994
	5.17	0.092	86.52 ± 3.26	0.992	0.0016	92.34 ± 2.78	0.993
	8.12	0.068	69.83 ± 2.92	0.992	0.0014	75.19 ± 3.51	0.992

behaviors might be in relation with the existence forms of Pb(II) and the surface charges of N-Fe/OMC. Since lead exists in different species (Fig. S5a), it is mainly Pb^{2+} ions at pH < 7, whereas it transforms into $Pb(OH)^+$, $Pb(OH)_2$ and $Pb(OH)_3^-$ at pH > 7. The isoelectric point (pH_{ZPC}) of N-Fe/OMC was 3.62 (Fig. S5b), which indicated that N-Fe/OMC became protonated and showed a positive net charge on its surface at pH 3.05, and thus, a significant electrostatic repulsion existed between the positively charged surface and the

cationic Pb(II) under this conditions. At pH > pH_{ZPC} (pH 5.17 or 8.12), the N-Fe/OMC surface was negatively charged. Meanwhile, Pb(II) existed in the style of Pb^{2+} and $Pb(OH)^{+}$, and consequently, cationic Pb(II) had access to the surface of N-Fe/OMC due to electrostatic attraction. Furthermore, the occurring of the chemical precipitation of Pb(II) ($Pb(OH)_2$) at higher solution pH (pH 8.12) also accelerated the removal of Pb(II).

On the other hand, neutral pH was more suitable for phenol adsorption (Fig. 6b). In the alkaline solution (pH 8.12), the surface of phenol easily revealed negatively charged because of the reaction with OH^{-}, while the net surface charge of N-Fe/OMC was negative, inconvenient for phenol adsorption. Furthermore, the competition from H^{+} was non-ignorable when the adsorption occurs at pH below the isoelectric point of N-Fe/OMC (pH 3.05). Thus, an eclectic pH (pH 5.17) catered to the uptake of phenol. In ordered to avoid the chemical precipitation of Pb(II) and simultaneously obtain high sorption efficiencies, pH 7.0 was selected eclectically to perform Pb(II) and phenol adsorption in other procedures.

3.4. Effect of ionic strength

The effect of ionic strength was investigated to explore the interaction mechanisms between Pb(II) and phenol with N-Fe/OMC. The sorption efficiencies of Pb(II) slightly decreased with the increase of NaCl concentration (Fig. 6c). The phenomenon could be explained by that Pb(II) would shape electrical double-layer complexes with N-Fe/OMC, and thus the adsorption would be hindered as the strong-electrolyte NaCl concentration increased. This was consistent with an ion-exchange mechanism since the adsorption interaction between the functional groups of N-Fe/OMC and Pb(II) was mainly ionic [33]. In addition, the contact between Pb(II) and N-Fe/OMC surface was limited since the activity coefficient of Pb(II) was affected by the solution ionic strength. The electrostatic repulsion between adsorbents with adsorbates increased as the ionic strength increased, and thus the available adsorption sites for Pb(II) decreased because of the competition of Na^{+} ions. Whereas the decrease was limited, which was probably due to that in addition to direct adsorption on the surface of N-Fe/OMC, the chemical surface complexation between Pb(II) and —NH_2 or —NH groups occurred and also conduced to the removal of Pb(II).

However, it is different for phenol adsorption. Generally, if phenol was adsorbed onto N-Fe/OMC by the dissociated anion forms, cationic Na^{+} in NaCl would pair with the negative adsorbates and the ionic repulsion among substances adsorbed on the surface of N-Fe/OMC would be reduced on the basis of the electrostatic forces theory. Thus, the adsorption capacity would increase with the increase of additional NaCl concentration. But in fact, change in NaCl concentration had little effect on the uptake of phenol. This implied that phenol was probably adsorbed onto N-Fe/OMC in the pattern of molecule, which did not possess charges. Thus, phenol adsorption was not predominated by electrostatic interaction, and it was mainly a physical combination process between phenol and N-Fe/OMC [4]. This was also the reason why the coexistence of high Pb(II) concentration had no obvious impact on phenol adsorption. Besides, another non-ignorable phenomenon was that the adsorption equilibrium was reached in longer time (150 min) with more NaCl (0.1 mol/L), and in shorter time (60 min) with less NaCl (0.001 mol/L). The possible reason was that at lower NaCl concentration, the water cluster was formed on the surface of N-Fe/OMC by hydrogen bonding with H_2O molecule, which could interface and accelerate phenol adsorption. However, the water cluster would be destroyed at higher NaCl concentration, and consequently extended the equilibrium time. Thus, phenol adsorption onto N-Fe/OMC only replied on those small handy phenol molecules, and in this way, the adsorption was delayed.

3.5. Thermodynamic of adsorption

Pb(II) adsorption as a function of contact time in three different temperatures is shown in Fig. 6e. The results showed that after adsorption equilibrium, the residual percentages of Pb(II) were 24.8%, 16.9% and 11.2% at 25 °C, 35 °C and 45 °C, respectively. The equilibrium could be reached within 30 min at 45 °C, whereas 90 min at 25 °C. The variation might be due to it that the mobility of Pb(II) and the active adsorption sites increased with the increase of temperature, which made more Pb(II) acquire sufficient energy to interact with active adsorption sites on the surface of N-Fe/OMC. Similar results for Pb(II) adsorption on iron oxide nanoparticles immobilized *Phanerochaete chrysosporium* [44], carbon nanotubes [36] and activated bentonite [45] had been reported.

However, the uptake capacities of phenol decreased as temperature increased (Fig. 6f). The phenomenon might be related with the weakening of adsorptive forces between the active adsorption sites of N-Fe/OMC and phenol. Besides, the tendency of phenol to escape the surface of the adsorbent significantly increased with the increase of temperature, which resulted in a reduction in boundary layer thickness, and thus lowered the adsorption of phenol. Similar trends had also been observed for phenol adsorption onto organomodified tirebolu bentonite [46], natural zeolites [47] and activated carbon prepared from tobacco residues [48].

Thermodynamics were utilized to evaluate the adsorption behaviors of N-Fe/OMC, and the corresponding equations are expressed as Eqs. (5), (6):

$$\ln\left(\frac{Q_e}{C_e}\right) = \frac{\Delta S^0}{R} - \frac{\Delta H^0}{RT} \tag{5}$$

$$\Delta G^0 = \Delta H^0 - T\Delta S^0 \tag{6}$$

where R is the gas constant (8.314 J/mol/K), T is the absolute temperature (K), and ΔS (J/mol/K), ΔH (kJ/mol) and ΔG (kJ/mol) are the changes in the entropy, enthalpy and Gibb's free energy of the system, respectively. The calculated parameters were shown in Table 5. It indicated that all ΔG^0 values towards Pb(II) and phenol adsorption were negative, indicating that the uptake of Pb(II) and phenol were spontaneous at these temperatures [33]. For Pb(II), the positive ΔH^0 (39.13 kJ/mol) confirmed the endothermic nature of adsorption. While the positive ΔS^0 (144.03 J/mol/K) suggested that increased randomness at the solid solution interface occurred in the internal structure of the uptake of Pb(II) onto N-Fe/OMC. For phenol, on the other hand, the negative ΔH^0 and ΔS^0 suggested that the exothermic nature of adsorption and the decreasing of randomness at the solid/liquid interface during phenol adsorption, respectively [49].

3.6. Proposed mechanisms of Pb(II) and phenol adsorption

On the basis of all information obtained above, a possible reaction mechanism for Pb(II) and phenol adsorption onto N-Fe/OMC was proposed in Fig. 7. In single system, Pb(II) was removed in two ways: direct adsorption onto the ordered mesoporous carbon pores and iron nanoparticles as well as complexation with amino groups of N-Fe/OMC [27], however phenol was removed only by adsorption on the surface of ordered mesoporous carbons [29]. In binary system, apart from the above conditions, there probably occurred another pollutants removal pathway that Pb(II) firstly chelated with phenol molecules, shaping the Pb(II)–phenol complexes [3]. Then the new complexes were directly adsorbed onto N-Fe/OMC or chelated with —NH and —NH_2.

Table 5
Thermodynamic parameters for Pb(II) and phenol adsorption on N-Fe/OMC.

Temperature (°C)	Pb(II)				Phenol			
	ΔS (J/K/mol)	ΔH (kJ/mol)	ΔG (kJ/mol)	R^2	ΔS (J/K/mol)	ΔH (kJ/mol)	ΔG (kJ/mol)	R^2
25	144.03	39.13	−4.53	0.999	−103.37	−39.30	−7.95	0.937
35			−5.97				−6.92	
45			−7.41				−5.88	

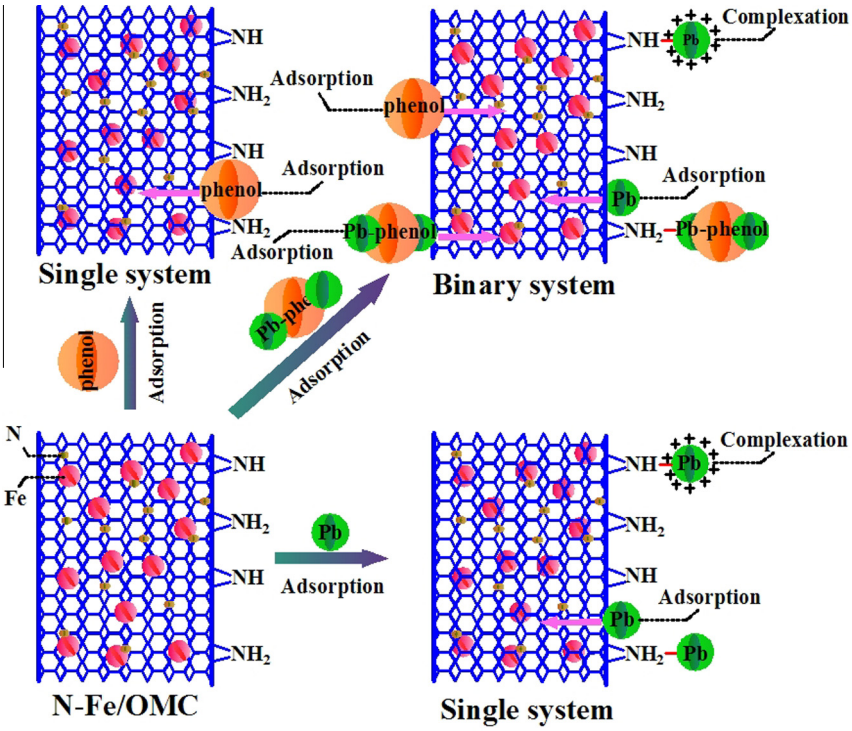

Fig. 7. Schematic diagram of the removal mechanism of Pb(II) and phenol adsorption onto N-Fe/OMC.

3.7. Regeneration of N-Fe/OMC

The regeneration investigation was carried out in seven consecutively adsorption–desorption cycles (Fig. 8). The sorption efficiencies declined slightly with the cycles, but it remained at high level with above 75% for Pb(II) and 84% for phenol in the seventh cycle. The regeneration and reuse performance of N-Fe/OMC was similar with the results of polyamine chelating resin for uptake of copper and *p*-nitrophenol [8], and magnetic multi-walled carbon nanotube for adsorption of atrazine and Cu(II) [50] in previous studies, indicating the excellent adsorption stability of the resultant sample. Therefore, in consideration of its magnetic separation and eminent regeneration abilities, N-Fe/OMC might offer an effective treatment to remove heavy metals and organics in more complex environments by in-situ regeneration and reuse.

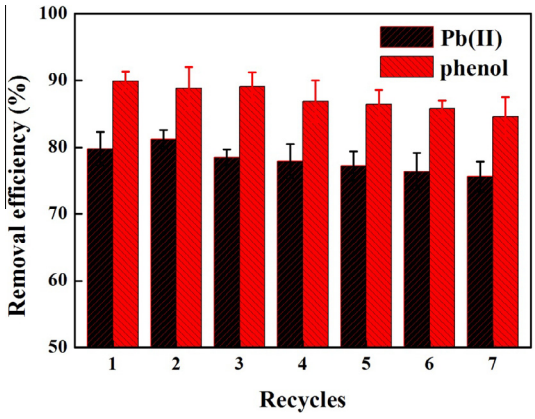

Fig. 8. Seven consecutive adsorption–desorption cycles of N-Fe/OMC for Pb(VI) and phenol. Initial Pb(II) and phenol concentrations of 50 mg/L and 50 mg/L, respectively, adsorbent dose of 5 mg, pH 7.0, temperature of 30 ± 1 °C, contact time of 240 min and ionic strength of 0.01 mol/L NaCl.

3.8. Application in real water samples

N-Fe/OMC was applied to treat real water samples including tap water, river water and landfill leachate to investigate its practical application (Table 6). The uptake capacities towards Pb(II) in tap water, river water and landfill leachate were slightly lower than ultrapure water because there existed many common cations, such as Na^+, K^+, Ca^{2+}, Mg^{2+} in the former three waters. These cations not only impacted ionic strength, aggrandizing the contact difficulty between Pb(II) and N-Fe/OMC, but also occupied the adsorption sites of N-Fe/OMC. The Pb(II) uptake amount in landfill leachate was a little higher than tap water and river water because plentiful organic matters in landfill leachate, such as humic acid and phenolic organics chelated with Pb(II), and thus improved Pb(II) adsorption. The phenol adsorption capacities in tap water and river water were nearly equal, higher than landfill leachate. The result again demonstrated that ionic strength hardly affected phenol uptake,

Table 6
The Pb(II) and phenol adsorption efficiencies of N-Fe/OMC in the single or binary system under four different real water samples.

Adsorption capacity (mg/g)	Adsorbates	Ultrapure water		Tap water		River water		Landfill leachate	
		Pb(II)	Phenol	Pb(II)	Phenol	Pb(II)	Phenol	Pb(II)	Phenol
Single system	5 mg/L Pb(II)/phenol	9.4 ± 0.52	9.7 ± 0.54	9.0 ± 0.35	9.5 ± 0.42	8.7 ± 0.51	9.3 ± 0.65	9.2 ± 0.71	8.7 ± 0.15
	10 mg/L Pb(II)/phenol	18.2 ± 0.98	19.2 ± 1.02	16.8 ± 1.09	18.6 ± 1.15	16.4 ± 0.89	18.3 ± 0.97	17.7 ± 1.18	16.0 ± 1.08
	50 mg/L Pb(II)/phenol	79.2 ± 5.42	89.9 ± 4.81	74.2 ± 5.41	88.5 ± 5.54	70.2 ± 5.24	86.1 ± 4.79	74.8 ± 4.19	71.4 ± 6.2
	100 mg/L Pb(II)/phenol	118.1 ± 9.54	141.2 ± 11.25	102.2 ± 10.25	140.1 ± 6.54	96.4 ± 7.42	138.6 ± 8.45	112.8 ± 15.24	101.1 ± 11.28
Binary system	5 mg/L Pb(II)+5 mg/L phenol	9.5 ± 0.25	9.9 ± 0.45	9.3 ± 0.29	9.7 ± 0.31	9.1 ± 0.29	9.4 ± 0.48	9.3 ± 0.59	8.8 ± 0.18
	10 mg/L Pb(II)+10 mg/L phenol	18.8 ± 0.51	19.6 ± 0.98	17.4 ± 0.84	19.1 ± 0.82	17.1 ± 1.02	18.5 ± 1.12	17.9 ± 0.95	16.5 ± 0.84
	50 mg/L Pb(II)+50 mg/L phenol	75.2 ± 3.98	87.5 ± 3.97	64.8 ± 4.25	86.1 ± 4.57	60.4 ± 5.25	84.6 ± 6.15	72.5 ± 3.24	69.7 ± 4.18
	100 mg/L Pb(II)+100 mg/L phenol	92.2 ± 4.25	137.5 ± 6.54	76.4 ± 8.51	134.6 ± 10.24	72.8 ± 6.84	133.4 ± 8.57	87.2 ± 7.21	95.2 ± 5.42

and the low adsorption capacity in landfill leachate could be explained by that the organic components possessing similar physicochemical properties with phenol would compete with phenol for the adsorption sites on N-Fe/OMC in landfill leachate. Thus, the phenol adsorption had been largely decreased.

4. Conclusions

In the present study, a newly nitrogen-functionalized magnetic ordered mesoporous carbon (N-Fe/OMC) was successfully prepared for removal of Pb(II) and phenol contamination from water. The functional material showed an excellent magnetic property and hydrophilicity, fast adsorption rate and high adsorption efficiency for the two target pollutants. Pb(II) was removed by direct adsorption onto the ordered mesoporous carbon pores and iron nanoparticles as well as complexation with amino groups of N-Fe/OMC, whereas phenol was eliminated only by direct adsorption. Pb(II) adsorption was a spontaneous and endothermic procedure, however phenol was an exothermic process. The mutual effects of coexisting Pb(II) and phenol on adsorption of each other revealed partial complexation and competition between Pb(II) and phenol. The regeneration indicated the excellent adsorption stability and good reutilization of N-Fe/OMC.

Acknowledgments

The study was financially supported by the Young Top-Notch Talent Support Program of China (2012), the National Natural Science Foundation of China (51222805), the Program for New Century Excellent Talents in University from the Ministry of Education of China (NCET-11-0129), Interdisciplinary Research Project of Hunan University, China Scholarship Council (CSC) (2010843195), the Fundamental Research Funds for the Central Universities, Hunan University, Foundation for the Author of Excellent Doctoral Dissertation of Hunan Province, the scientific Research Fund of Hunan Provincial Education Department (13C1082).

Appendix A. Supplementary data

Supplementary data associated with this article can be found, in the online version, at http://dx.doi.org/10.1016/j.cej.2014.08.081.

References

[1] G.X. Yang, H. Jiang, Amino modification of biochar for enhanced adsorption of copper ions from synthetic wastewater, Water Res. 48 (2014) 396–405.
[2] E. Saputra, S. Muhammad, H.Q. Sun, H.M. Ang, M.O. Tadé, S.B. Wang, Different crystallographic one-dimensional MnO_2 nanomaterials and their superior performance in catalytic phenol degradation, Environ. Sci. Technol. 47 (2013) 5882–5887.
[3] S.B. Yang, J. Hu, C.L. Chen, D.D. Shao, X.K. Wang, Mutual effects of Pb(II) and humic acid adsorption on multiwalled carbon nanotubes/polyacrylamide composites from aqueous solutions, Environ. Sci. Technol. 45 (2011) 3621–3627.
[4] G.C. Chen, X.Q. Shan, Y.S. Wang, B. Wen, Z.G. Pei, Y.N. Xie, T. Liu, J.J. Pignatello, Adsorption of 2,4,6-trichlorophenol by multi-walled carbon nanotubes as affected by Cu(II), Water Res. 43 (2009) 2409–2418.
[5] P. Luo, Y.F. Zhao, B. Zhang, J.D. Liu, Y. Yang, J.F. Liu, Study on the adsorption of neutral red from aqueous solution onto halloysite nanotubes, Water Res. 44 (2010) 1489–1497.
[6] L.M. Pastrana-Martínez, M.V. López-Ramón, M.A. Fontecha-Cámara, C. Moreno-Castilla, Batch and column adsorption of herbicide fluroxypyr on different types of activated carbons from water with varied degrees of hardness and alkalinity, Water Res. 44 (2010) 879–885.
[7] G.D. Yang, L. Tang, X.X. Lei, G.M. Zeng, Y. Cai, X. Wei, Y.Y. Zhou, S.S. Li, Y. Fang, Y. Zhang, Cd(II) removal from aqueous solution by adsorption on α-ketoglutaric acid-modified magnetic chitosan, Appl. Surf. Sci. 292 (2014) 710–716.
[8] T.P. Chen, F.Q. Liu, C. Ling, J. Gao, C. Xu, L.J. Li, A.M. Li, Insight into highly efficient co-removal of copper and p-nitrophenol by a newly synthesized polyamine chelating resin from aqueous media: competition and enhancement effect upon site recognition, Environ. Sci. Technol. 47 (2013) 13652–13660.
[9] Z.B. Lei, X.X. Sun, H.J. Wang, Z.H. Liu, X.S. Zhao, Platelet CMK-5 as an excellent mesoporous carbon to enhance the pseudocapacitance of polyaniline, ACS Appl. Mater. Interfaces 5 (2013) 7501–7508.
[10] L. Tang, Y.Y. Zhou, G.M. Zeng, Z. Li, Y.Y. Liu, Y. Zhang, G.Q. Chen, G.D. Yang, X.X. Lei, M.S. Wu, A tyrosinase biosensor based on ordered mesoporous carbon–Au/L-lysine/Au nanoparticles for simultaneous determination of hydroquinone and catechol, Analyst 138 (2013) 3552–3560.
[11] B. Yuan, X.F. Wu, Y.X. Chen, J.H. Huang, H.M. Luo, S.G. Deng, Adsorption of CO_2, CH_4, and N_2 on ordered mesoporous carbon: approach for greenhouse gases capture and biogas upgrading, Environ. Sci. Technol. 47 (2013) 5474–5480.
[12] J. Tang, T. Wang, X.C. Pan, X. Sun, X.L. Fan, Y.X. Guo, H.R. Xue, J.P. He, Synthesis and electrochemical characterization of N-doped partially graphitized ordered mesoporous carbon-Co composite, J. Phys. Chem. C 117 (2013) 16896–16906.
[13] H.W. Liang, W. Wei, Z.S. Wu, X.L. Feng, K. Müllen, Mesoporous metal-nitrogen-doped carbon electrocatalysts for highly efficient oxygen reduction reaction, J. Am. Chem. Soc. 135 (2013) 16002–16005.
[14] Z.X. Wu, Y.Y. Lv, Y.Y. Xia, P.A. Webley, D.Y. Zhao, Ordered mesoporous platinum@graphitic carbon embedded nanophase as a highly active, stable, and methanol-tolerant oxygen reduction electrocatalyst, J. Am. Chem. Soc. 134 (2012) 2236–2245.
[15] Y.D. Xia, R. Mokaya, Synthesis of ordered mesoporous carbon and nitrogen-doped carbon materials with graphitic pore walls via a simple chemical vapor deposition method, Adv. Mater. 16 (2004) 1553–1558.

[16] D.S. Yang, D. Bhattacharjya, M.Y. Song, J.S. Yu, Highly efficient metal-free phosphorus-doped platelet ordered mesoporous carbon for electrocatalytic oxygen reduction, Carbon 67 (2014) 736–743.
[17] L. Tang, G.D. Yang, G.M. Zeng, Y. Cai, S.S. Li, Y.Y. Zhou, Y. Pang, Y.Y. Liu, Y. Zhang, B. Luna, Synergistic effect of iron doped ordered mesoporous carbon on adsorption-coupled reduction of hexavalent chromium and the relative mechanism study, Chem. Eng. J. 239 (2014) 114–122.
[18] K.K.R. Datta, B.V.S. Reddy, K. Ariga, A. Vinu, Gold nanoparticles embedded in a mesoporous carbon nitride stabilizer for highly efficient three-component coupling reaction, Angew. Chem. Int. Ed. 49 (2010) 5961–5965.
[19] J.K. Dombrovskis, H.Y. Jeong, K. Fossum, O. Terasaki, A.E.C. Palmqvist, Transition metal ion-chelating ordered mesoporous carbons as noble metal-free fuel cell catalysts, Chem. Mater. 25 (2013) 856–861.
[20] D.Y. Zhao, J.L. Feng, Q.S. Huo, N.G. Melosh, H. Fredrickson, B.F. Chmelka, G.D. Stucky, Triblock copolymer syntheses of mesoporous silica with periodic 50–300 angstrom pores, Science 279 (1998) 548–552.
[21] X.F. Wang, P. Liu, Y. Tian, L.Q. Zang, Novel synthesis of Fe-containing mesoporous carbons and their release of ibuprofen, Microporous Mesoporous Mater. 145 (2011) 98–103.
[22] S.J. Shrestha, S.S. Asheghi, J. Timbro, W.E. Mustain, Effects of pore structure in nitrogen functionalized mesoporous carbon on oxygen reduction reaction activity of platinum nanoparticles, Carbon 60 (2013) 28–40.
[23] N.N. Liu, L.W. Yin, C.X. Wang, L.Y. Zhang, N. Lun, D. Xiang, Y.X. Qi, R. Gao, Adjusting the texture and nitrogen content of ordered mesoporous nitrogen-doped carbon materials prepared using SBA-15 silica as a template, Carbon 48 (2010) 3579–3591.
[24] Y. Pang, G.M. Zeng, L. Tang, Y. Zhang, Y.Y. Liu, X.X. Lei, Z. Li, J.C. Zhang, G.X. Xie, PEI-grafted magnetic porous powder for highly effective adsorption of heavy metal ions, Desalination 281 (2011) 278–284.
[25] Y. Chi, W.C. Geng, L. Zhao, X. Yan, Q. Yuan, N. Li, X.T. Li, Comprehensive study of mesoporous carbon functionalized with carboxylate groups and magnetic nanoparticles as a promising adsorbent, J. Colloid Interface Sci. 369 (2012) 366–372.
[26] V.K. Gupta, S. Agarwal, T.A. Saleh, Chromium removal by combining the magnetic properties of iron oxide with adsorption properties of carbon nanotubes, Water Res. 45 (2011) 2207–2212.
[27] X.L. Wang, L. Shu, Y.Q. Wang, B.B. Xu, Y.C. Bai, S. Tao, B.S. Xing, Sorption of peat humic acids to multi-walled carbon nanotubes, Environ. Sci. Technol. 45 (2011) 9276–9283.
[28] N. Pitakteeratham, A. Hafuka, H. Satoh, Y. Watanabe, High efficiency removal of phosphate from water by zirconium sulfate-surfactant micelle mesostructure immobilized on polymer matrix, Water Res. 47 (2013) 3583–3590.
[29] A. Bahdod, S.E. Asri, A. Saoiabi, T. Coradin, A. Laghzizil, Adsorption of phenol from an aqueous solution by selected apatite adsorbents: kinetic process and impact of the surface properties, Water Res. 43 (2009) 313–318.
[30] Z.H. Huang, X.Y. Zheng, W. Lv, M. Wang, Q.H. Yang, F.Y. Kang, Adsorption of lead(II) ions from aqueous solution on low-temperature exfoliated graphene nanosheets, Langmuir 27 (2011) 7558–7562.
[31] Y. Liu, Z.C. Liu, J. Gao, J.D. Dai, J. Han, Y. Wang, J.M. Xie, Y.S. Yan, Selective adsorption behavior of Pb(II) by mesoporous silica SBA-15-supported Pb(II)-imprinted polymer based on surface molecularly imprinting technique, J. Hazard. Mater. 186 (2011) 197–205.
[32] E. Eren, H. Gumus, Characterization of the structural properties and Pb(II) adsorption behavior of iron oxide coated sepiolite, Desalination 273 (2011) 276–284.
[33] I. Vergili, G. Soltobaeva, Y. Kaya, Z.B. Gonder, S. Çavuş, G. Gurdag, Study of the removal of Pb(II) using a weak acidic cation resin: kinetics, thermodynamics, equilibrium, and breakthrough curves, Ind. Eng. Chem. Res. 52 (2013) 9227–9238.
[34] D.H.K. Reddy, S.M. Lee, Three-dimensional porous spinel ferrite as an adsorbent for Pb(II) removal from aqueous solutions, Ind. Eng. Chem. Res. 52 (2013) 15789–15800.
[35] W.H. Zou, R.P. Han, Z.Z. Chen, J. Shi, H.M. Liu, Characterization and properties of manganese oxide coated zeolite as adsorbent for removal of copper(II) and lead(II) ions from solution, J. Chem. Eng. Data 51 (2006) 534–541.
[36] X. Zhao, Q. Jia, N. Song, W. Zhou, Y. Li, Adsorption of Pb(II) from an aqueous solution by titanium dioxide/carbon nanotube nanocomposites: kinetics, thermodynamics, and isotherms, J. Chem. Eng. Data 55 (2010) 4428–4433.
[37] J.Q. Nie, Q. Zhang, M.Q. Zhao, J.Q. Huang, Q. Wen, Y. Cui, W.Z. Qian, F. Wei, Synthesis of high quality single-walled carbon nanotubes on natural sepiolite and their use for phenol absorption, Carbon 49 (2011) 1568–1580.
[38] K.M. Parida, A.C. Pradhan, Removal of phenolic compounds from aqueous solutions by adsorption onto manganese nodule leached residue, J. Hazard. Mater. 173 (2010) 758–764.
[39] H.L. Parker, V.L. Budarin, J.H. Clark, A.J. Hunt, Use of starbon for the adsorption and desorption of phenols, ACS Sustainable Chem. Eng. 1 (2013) 1311–1318.
[40] M. Kilic, E.A. Varol, A.E. Putun, Adsorptive removal of phenol from aqueous solutions on activated carbon prepared from tobacco residues: equilibrium, kinetics and thermodynamics, J. Hazard. Mater. 189 (2011) 397–403.
[41] Y.F. Zhu, L.X. Zhang, F.M. Schappacher, R. Pöttgen, J.L. Shi, S. Kaskel, Synthesis of magnetically separable porous carbon microspheres and their adsorption properties of phenol and nitrobenzene from aqueous solution, J. Phys. Chem. C 112 (2008) 8623–8628.
[42] Y.F. Zhu, E. Kockrick, S. Kaskel, T. Ikoma, N. Hanagata, Nanocasting route to ordered mesoporous carbon with FePt nanoparticles and its phenol adsorption property, J. Phys. Chem. C 113 (2009) 5998–6002.
[43] A.G. Plaska, M. Majdan, S. Pikus, D. Sternik, Simultaneous adsorption of chromium(VI) and phenol on natural red clay modified by HDTMA, Chem. Eng. J. 179 (2012) 140–150.
[44] P. Xu, G.M. Zeng, D.L. Huang, C. Lai, M.H. Zhao, Z. Wei, N.J. Li, C. Huang, G.X. Xie, Adsorption of Pb(II) by iron oxide nanoparticles immobilized *Phanerochaete chrysosporium*: equilibrium, kinetic, thermodynamic and mechanisms analysis, Chem. Eng. J. 203 (2012) 423–431.
[45] A.R. Kula, H. Koyuncu, Adsorption of Pb(II) from aqueous solution by native and activated bentonite: kinetic, equilibrium and thermodynamic study, J. Hazard. Mater. 179 (2010) 332–339.
[46] H.B. Senturk, D. Ozdes, A. Gundogdu, C. Duran, M. Soylak, Removal of phenol from aqueous solutions by adsorption onto organomodified tirebolu bentonite: equilibrium, kinetic and thermodynamic study, J. Hazard. Mater. 172 (2009) 353–362.
[47] R.I. Yousef, B.E. Eswed, A.H.A. Muhtaseb, Adsorption characteristics of natural zeolites as solid adsorbents for phenol removal from aqueous solutions: kinetics, mechanism, and thermodynamics studies, Chem. Eng. J. 171 (2011) 1143–1149.
[48] M. Kilic, E.A. Varol, A.E. Pütün, Adsorptive removal of phenol from aqueous solutions on activated carbon prepared from tobacco residues: equilibrium, kinetics and thermodynamics, J. Hazard. Mater. 189 (2011) 397–403.
[49] V.K. Gupta, N. Atar, M.L. Yola, Z. Üstündağ, L. Uzun, A novel magnetic Fe@Au core shell nanoparticles anchored graphene oxide recyclable nanocatalyst for the reduction of nitrophenol compounds, Water Res. 48 (2014) 210–217.
[50] W.W. Tang, G.M. Zeng, J.L. Gong, Y. Liu, X.Y. Wang, Y.Y. Liu, Z.F. Liu, L. Chen, X.R. Zhang, D.Z. Tu, Simultaneous adsorption of atrazine and Cu(II) from wastewater by magnetic multi-walled carbon nanotube, Chem. Eng. J. 211–212 (2012) 470–478.